Hybrid Quantum Circuit with a Superconducting Qubit Coupled to a Spin Ensemble

Y. Kubo,[1] C. Grezes,[1] A. Dewes,[1] T. Umeda,[2] J. Isoya,[2] H. Sumiya,[3] N. Morishita,[4] H. Abe,[4] S. Onoda,[4] T. Ohshima,[4] V. Jacques,[5] A. Dréau,[5] J.-F. Roch,[5] I. Diniz,[6] A. Auffeves,[6] D. Vion,[1] D. Esteve,[1] and P. Bertet[1]

[1]*Quantronics group, SPEC (CNRS URA 2464), IRAMIS, DSM, CEA-Saclay, 91191 Gif-sur-Yvette, France*
[2]*Research Center for Knowledge Communities, University of Tsukuba, Tsukuba 305-8550, Japan*
[3]*Sumitomo Electric Industries Ltd., Itami 664-001, Japan*
[4]*Japan Atomic Energy Agency, Takasaki 370-1292, Japan*
[5]*LPQM (CNRS UMR 8537), ENS de Cachan, 94235 Cachan, France*
[6]*Institut Néel, CNRS, BP 166, 38042 Grenoble, France*

(Received 19 October 2011; published 21 November 2011)

We report the experimental realization of a hybrid quantum circuit combining a superconducting qubit and an ensemble of electronic spins. The qubit, of the transmon type, is coherently coupled to the spin ensemble consisting of nitrogen-vacancy centers in a diamond crystal via a frequency-tunable superconducting resonator acting as a quantum bus. Using this circuit, we prepare a superposition of the qubit states that we store into collective excitations of the spin ensemble and retrieve back into the qubit later on. These results constitute a proof of concept of spin-ensemble based quantum memory for superconducting qubits.

DOI: 10.1103/PhysRevLett.107.220501 PACS numbers: 03.67.Lx, 42.50.Ct, 42.50.Pq, 85.25.Cp

Present-day implementations of quantum information processing rely on two widely different types of quantum bits (qubits). On the one hand, microscopic systems such as atoms or spins are naturally well decoupled from their environment and as such can reach extremely long coherence times [1,2]; on the other hand, more macroscopic objects such as superconducting circuits are strongly coupled to electromagnetic fields, making them easy to entangle [3,4] although with shorter coherence times [5,6]. It thus seems appealing to combine the two types of systems in hybrid structures that could possibly take the best of both worlds.

But if superconducting qubits have been successfully coupled to electromagnetic [7] as well as mechanical [8] resonators, coupling them to microscopic systems in a controlled way has up to now remained an elusive perspective—even though qubits sometimes turn out to be coupled to unknown and uncontrolled microscopic degrees of freedom with relatively short coherence times [9]. Whereas the coupling constant g of one individual microscopic system to a superconducting circuit is usually too weak for quantum information applications, ensembles of N such systems are coupled with a constant $g\sqrt{N}$ enhanced by collective effects. This makes possible to reach a regime of strong coupling between one collective variable of the ensemble and the circuit. This collective variable, which behaves in the low excitation limit as a harmonic oscillator, has been proposed [10–13] as a quantum memory for storing the state of superconducting qubits. Experimentally, the strong coupling between an ensemble of electronic spins and a superconducting resonator has been demonstrated spectroscopically [14–16], and the storage of a microwave field into collective excitations of a spin ensemble has been observed very recently [17,18]. These experiments were however carried out in a classical regime since the resonator and spin ensemble behaved as two coupled harmonic oscillators driven by large microwave fields. In the perspective of building a quantum memory, it is instead necessary to perform experiments at the level of a single quantum of excitation. For that purpose, we integrate on the same chip three different quantum systems: an ensemble of electronic spins, a superconducting qubit, and a resonator acting as a quantum bus between the qubit and the spins. A sketch of the experiment is shown in Fig. 1.

The spin ensemble N-V consists of $\sim 10^{11}$ negatively charged nitrogen vacancy (NV) color centers [19] in a diamond crystal. These centers have an electronic spin $S = 1$, with electron spin resonance (ESR) transition frequencies $\omega_{\pm}/2\pi \simeq 2.88$ GHz between energy levels $m_S = 0$ and $m_S = \pm 1$ in zero magnetic field [see Fig. 1(c)]. The electronic spin of the NV center is further coupled by hyperfine (HF) interaction to the spin-one ^{14}N nucleus, which splits $\omega_{\pm}$ into three peaks separated by 2.2 MHz [20,21]. In our experiment, the diamond crystal is glued on top of the chip, and the degeneracy between states $m_S = \pm 1$ is lifted with a $B_{\mathrm{NV}} = 1.4$ mT magnetic field applied parallel to the chip and along the [1, 1, 1] crystalline axis. The NV frequencies being sensitive only to the projection of B_{NV} along the NV axis, two groups of NVs thus experience different Zeeman effects: those along [1,1,1] (denoted I) and those along either of the three other $\langle 1, 1, 1\rangle$ axes (denoted III as they are 3 times more numerous). This results in four different ESR frequencies $\omega_{\pm \mathrm{I}, \pm \mathrm{III}}$.

The qubit Q is a Cooper-pair box of the transmon type [5,22] with transition frequency ω_Q between its ground

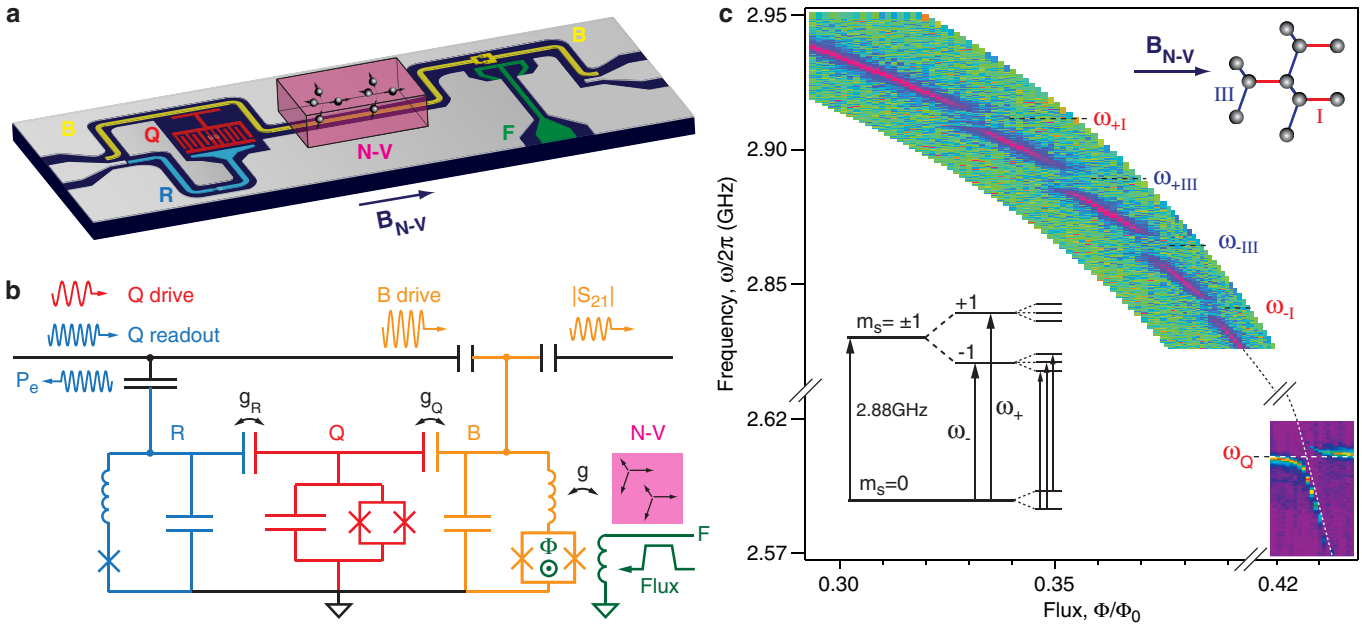

FIG. 1 (color online). Description of the hybrid quantum circuit demonstrated in this work. (a),(b) Three-dimensional sketch of the device and corresponding electrical scheme. The ensemble N-V of electronic spins (magenta) consists of 10^{11} NV centers in a diamond crystal glued on the chip surface. The transmon qubit Q (in red) is capacitively coupled to a resonator R (in blue) made nonlinear with a Josephson junction and used to readout its state. The bus B (in yellow) is electrostatically coupled to Q and magnetically coupled to N-V. Bus B contains a SQUID that makes its frequency $\omega_B(\Phi)$ tunable by applying in its loop a flux Φ via a fast on-chip current line F (in green). A magnetic field B_{NV} is applied parallel to the [1,1,1] crystallographic axis. (c), (lower left inset) Energy level structure of NV centers. Transitions between $m_S = 0$ and $m_S = \pm 1$ at frequency $\omega_\pm$ are further split in three resonance lines due to the hyperfine interaction with the ^{14}N nuclear spin [20]. (main panel) Two-dimensional plot of the transmission $|S_{21}|(\omega, \Phi)$ through B in dB units, with Φ expressed in units of the superconducting flux quantum $\Phi_0 = h/2e$, for a field $B_{\mathrm{NV}} = 1.4$ mT applied to the spins. Color scale goes from -55 dB (background, green) to -30 dB (magenta). Four vacuum Rabi splittings are observed whenever ω_B matches one NV center resonance frequency. The four transition frequencies $\omega_{\pm\mathrm{I,III}}$ correspond to the two distinct families I and III of NV centers, aligned along the [1,1,1] crystal direction parallel to B_{NV} or along one of the three other possible $\langle 1, 1, 1\rangle$ axes, respectively (see upper right inset). (main panel, bottom right) Qubit excited state probability P_e as a function of the frequency of the exciting microwave and Φ. Color scale goes from 0.1 (background, purple) to 0.3 (yellow). When ω_B matches the qubit frequency $\omega_Q = 2.607$ GHz, the qubit spectrum shows an anticrossing demonstrating its coupling to B with constant $g_Q/2\pi = 7.2$ MHz.

state $|g\rangle$ and excited state $|e\rangle$. It is coupled to a nonlinear resonator R which is used to readout its state, as in related circuit quantum electrodynamics experiments [23]. Single-qubit rotations are realized by applying microwave pulses at ω_Q through R. Qubit state readout is performed by measuring the phase of a microwave pulse reflected on R, which depends on the qubit state; the probability P_e to find the qubit in $|e\rangle$ is then determined by repeating $\sim 10^4$ times the same experimental sequence.

The quantum bus B, a superconducting resonator with quality factor $\sim 10^4$, is electrostatically coupled to the qubit and magnetically coupled to the spin ensemble. In order to bridge the difference in frequency between Q and N-V, the bus frequency ω_B can be tuned on a nanosecond time scale [24] by applying current pulses through an on-chip flux line F, inducing a magnetic flux Φ through a SQUID embedded in B [21,25].

We first characterize our hybrid circuit by spectroscopic measurements. The NV frequencies and coupling constants are obtained by measuring the microwave transmission $|S_{21}(\omega)|$ through the bus, while scanning its frequency $\omega_B(\Phi)$ across the NV resonances. Vacuum Rabi splittings are observed when ω_B matches the ESR frequencies at $\omega_{+\mathrm{I}}/2\pi = 2.91$ GHz, $\omega_{-\mathrm{I}}/2\pi = 2.84$ GHz, $\omega_{+\mathrm{III}}/2\pi = 2.89$ GHz, and $\omega_{-\mathrm{III}}/2\pi = 2.865$ GHz (see Fig. 1). From the data we extract the coupling constants $g_{\pm\mathrm{I}}/2\pi = 2.9$ MHz and $g_{\pm\mathrm{III}}/2\pi = 3.8$ MHz, the difference between the two values resulting essentially from the larger number of NV centers in group III. Qubit spectroscopy is performed by scanning the frequency of a microwave pulse applied through R, and by measuring P_e, which yields $\omega_Q/2\pi = 2.607$ GHz. This spectroscopy, measured while scanning ω_B across ω_Q, shows an anticrossing [see Fig. 1(c)] that yields the coupling constant $g_Q/2\pi = 7.2$ MHz between Q and B.

Throughout the experiments reported in the following, the spins and qubit frequencies are kept fixed, and only ω_B is varied in order to transfer coherently quantum information between Q and N-V. For this purpose, a key operation is the qubit-bus SWAP gate that transfers an arbitrary qubit

state $\alpha|g\rangle + \beta|e\rangle$ into the corresponding photonic state $\alpha|0\rangle_B + \beta|1\rangle_B$ of the bus, leaving the qubit in $|g\rangle$. This SWAP gate could be performed by tuning ω_B in resonance with ω_Q for a duration $\pi/2g_Q$ [26]. Here we prefer instead to adiabatically sweep ω_B across ω_Q as this sequence is more immune to flux noise in the SQUID loop of B [21]. This adiabatic SWAP (aSWAP) achieves the same quantum operation as the resonant SWAP except for an irrelevant dynamical phase. The experiments then proceed by combining single-qubit rotations, aSWAP gates, and flux pulses placing B and N-V in and out of resonance for properly chosen interaction times τ.

We apply such a sequence with the qubit initially prepared in $|e\rangle$ (see Fig. 2). A first aSWAP converts $|e\rangle$ into the bus Fock state $|1\rangle_B$; B is brought in or near resonance with the spin ensemble for a duration τ; the resulting B state is then transferred back into the qubit, which is finally readout. Figure 2(b) shows the resulting curves $P_e(\tau)$ when the bus is brought in resonance either with $\omega_{-\mathrm{III}}$ or $\omega_{-\mathrm{I}}$. An oscillation in P_e is observed, revealing a storage in the spin ensemble of the single quantum of excitation initially in the qubit at $\tau_{s,\mathrm{III}} = 65$ ns or $\tau_{s,\mathrm{I}} = 97$ ns, and a retrieval back into the qubit at $\tau_{r,\mathrm{III}} = 116$ ns or $\tau_{r,\mathrm{I}} = 146$ ns. The fidelity of this storage-retrieval process, defined as

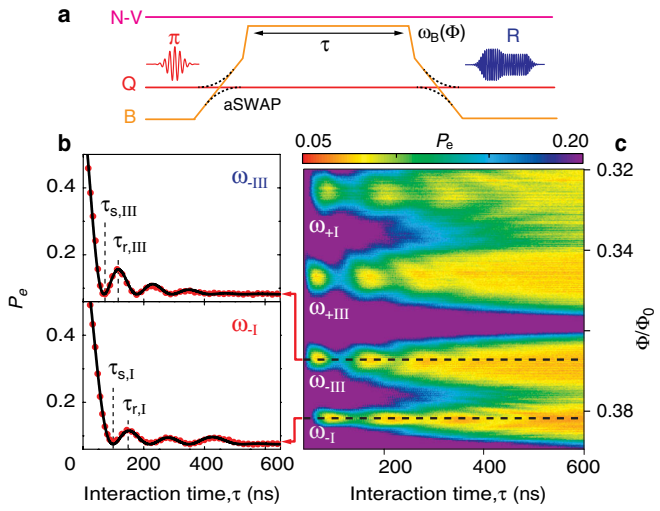

FIG. 2 (color online). Storage and retrieval of a single quantum of excitation from the qubit to the spin ensemble. (a), Experimental sequence showing the microwave pulses used for exciting the qubit in $|e\rangle$ (π pulse) and for reading it out (R pulse), as well as transition frequencies of the quantum bus (B), qubit (Q), and spins (N-V). (b), Experimental (red dots) and theoretical (black line—see text) probability $P_e(\tau)$ for ω_B tuned to $\omega_{-\mathrm{III}}$ (top) or $\omega_{-\mathrm{I}}$ (bottom), showing the storage and retrieval times τ_s and τ_r. (c), Two-dimensional plot of P_e versus interaction time τ and flux pulse height Φ, showing resonance with the four spin groups. Chevron-like patterns are observed, showing a faster oscillation with reduced amplitude when ω_B is detuned from the spin resonance, as expected. Note that the difference between the ω_- and ω_+ patterns in the same NV group is simply caused by the nonlinear dependence of ω_B on Φ [25].

$P_e(\tau_r)/P_e(0)$, is 0.14 for group III and 0.07 for group I. These relatively low values are not due to a short spin dephasing time, but rather to an interference effect caused by the HF structure of NV centers, as evidenced by the nonexponential damping observed in $P_e(\tau)$. These measurements are accurately reproduced by a full calculation of the spin-resonator dynamics [18,21,27,28] taking into account this HF structure, with the linewidth of each HF peak as the only adjustable parameter. A linewidth of 1.6 MHz is in this way determined for the spins in group I [21], and of 2.4 MHz for group III. This larger value is due to a residual misalignment of B_{NV} from the [1,1,1] crystalline axis causing each of the three $\langle 1, 1, 1\rangle$ NV orientations noncollinear with the field to experience slightly different Zeeman shifts. We finally note that in both curves shown in Fig. 2(b) $P_e(\tau)$ tends towards 0.08 at long times, as is also found with the qubit initially in $|g\rangle$. This proves that the collective spin variable coupled to B is, as requested for experiments in the quantum regime, in its ground state $|0\rangle_{-\mathrm{I},-\mathrm{III}}$ with a large probability $\sim$0.92 at equilibrium, which corresponds to a temperature of $\sim$50 mK. Varying both ω_B and τ with the same pulse sequence, we observe similar storage-retrieval cycles at all four spin frequencies [see Fig. 2(c)].

In addition to storing a single excitation from the qubit, one has to test if a coherent superposition of states can be transferred to the spin ensemble and retrieved. For that, we now perform the aSWAP and bring ω_B in resonance with $\omega_{-\mathrm{I}}$ after having prepared the qubit in $(|g\rangle + |e\rangle)/\sqrt{2}$ instead of $|e\rangle$, and we reconstruct the Bloch vector of the qubit by quantum state tomography at the end of the sequence (see Fig. 3). More precisely, we measure $\langle\sigma_X\rangle$, $\langle\sigma_Y\rangle$ and $\langle\sigma_Z\rangle$ by using $\pi/2$ rotations around Y, X, or no rotation at all (I) prior to qubit readout. After substracting a trivial rotation around Z occurring at frequency $(\omega_{-\mathrm{I}} - \omega_Q)$, we reconstruct the trajectory of this Bloch vector as a function of the interaction time τ. It is plotted in Fig. 3, together with the off-diagonal element ρ_{ge} of the final qubit density matrix, which quantifies its coherence. We find that no coherence is left in the qubit at the end of the sequence for $\tau = \tau_{s,\mathrm{I}}$, as expected for a full storage of the initial state into the ensemble. Then, coherence is retrieved at $\tau = \tau_{r,\mathrm{I}}$, although with an amplitude $\sim$5 times smaller than its value at $\tau = 0$ (i.e., without interaction with the spins). Note the π phase shift occurring after each storage-retrieval cycle, characteristic of 2π rotations in the two-level space $\{|1_B, 0_{-\mathrm{I}}\rangle, |0_B, 1_{-\mathrm{I}}\rangle\}$. The combination of the results of Figs. 2 and 3 demonstrates that superpositions of the two qubit states can be stored and retrieved in a spin ensemble—although with limited fidelity—and thus represents a proof-of-concept of a spin-based quantum memory for superconducting qubits.

To evaluate the time during which quantum coherence can be stored in the ensemble, we perform a Ramsey-like experiment on the spin ensemble at the single-photon level

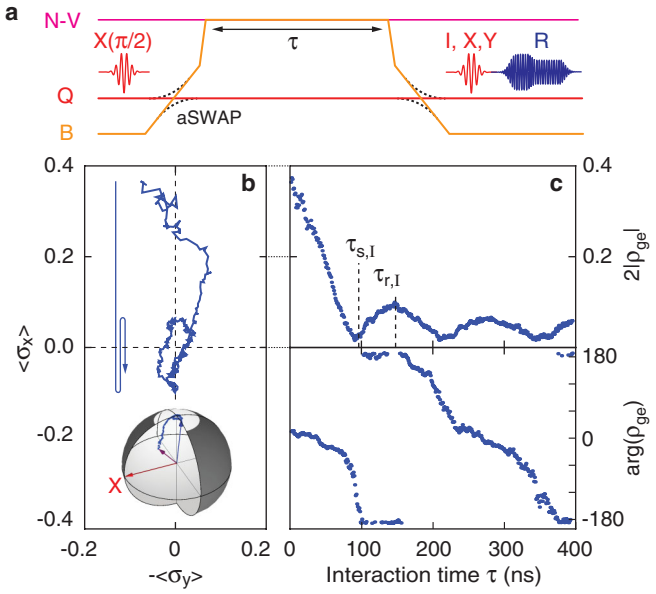

FIG. 3 (color online). Storage and retrieval of a coherent superposition of states from the qubit to the spin ensemble. (a) Experimental pulse sequence: the qubit is prepared by a $\pi/2$ pulse in state $(|g\rangle + |e\rangle)/\sqrt{2}$, which is transferred to B by an aSWAP. Bus B is then immediately tuned to $\omega_{-\mathrm{I}}/2\pi = 2.84$ GHz for an interaction time τ. The quantum state of B is then transferred back to the qubit by a second aSWAP. Quantum state tomography is finally performed to determine the qubit state by applying either I, X, or Y operation to the qubit. (b), Trajectory of the qubit Bloch vector on the Bloch sphere (bottom inset), and its projection on the equatorial plane. (c), Modulus and phase of the off-diagonal element ρ_{ge} of the qubit density matrix as a function of interaction time τ.

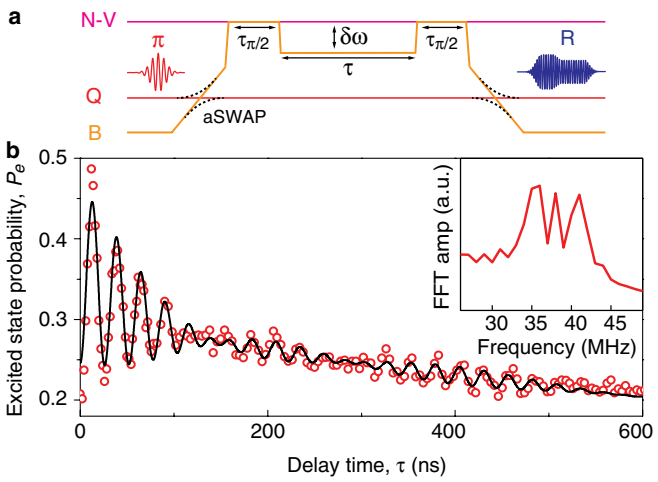

FIG. 4 (color online). Ramsey-like experiment on the spin ensemble at the single-photon level. (a), Experimental pulse sequence: the qubit is prepared in its excited state $|e\rangle$ by a π pulse; the state $|e, 0_B\rangle$ is then adiabatically transferred to $|g, 1_B\rangle$ by an aSWAP. A fast flux pulse subsequently brings ω_B onto $\omega_{-\mathrm{I}}$, and then lets B and the spins from group $-\mathrm{I}$ interact for half a swap time $\tau_{\pi/2} = \tau_{s,\mathrm{I}}/2$, generating an entangled state of the two systems. B is then detuned from the spins by $\delta\omega/2\pi = 38$ MHz during a time τ, and a second half-swap is performed. The quantum state of B is then transferred back to the qubit, which is finally readout. (b), Measured (red circles) and calculated (black line—see text) probability $P_e(\tau)$, as well as the Fourier transform of the experimental data (inset) revealing the NV centers HF structure.

(see Fig. 4): we initially prepare the qubit in $|e\rangle$, transfer its state to B, then tune ω_B to $\omega_{-\mathrm{I}}$ for a duration $\tau_{\pi/2} = \tau_{s,-\mathrm{I}}/2$, after which ω_B is suddenly detuned by $\delta\omega/2\pi = 38$ MHz for a time τ. At this point, the joint bus-spin ensemble state is an entangled state $(|1_B, 0_{-\mathrm{I}}\rangle + e^{i\varphi}|0_B, 1_{-\mathrm{I}}\rangle)/\sqrt{2}$ with a phase $\varphi = \delta\omega\tau$. Bus B is then put back in resonance with the spins for a second interaction of duration $\tau_{\pi/2}$ that converts the phase φ into population of $|1_B, 0_{-\mathrm{I}}\rangle$. This population is finally transferred to the qubit, and readout. Oscillations at frequency $\delta\omega$ are observed in $P_e(\tau)$ as seen in Fig. 4, confirming that the resonator and the spins are entangled after the first half-swap pulse. These oscillations are modulated by a beating pattern, with an overall damping of the oscillations envelope in ~200 ns. Quite remarkably, this beating observed in the qubit excited state probability is directly caused by the HF structure of NV centers, as proved by the Fourier transform of $P_e(\tau)$ which shows the three HF lines. The full calculation of the system dynamics quantitatively captures both the beatings and the oscillations damping, which is thus completely explained by the 1.6 MHz inhomogeneous linewidth of each HF line taken into account in the theory.

The previous results suggest that the storage of quantum information in the NV centers ensemble is at present limited both by its HF structure and by the inhomogeneous broadening of its resonance. This broadening is attributed to dipolar interactions between the NV centers and residual paramagnetic impurities (likely neutral nitrogen atoms) in the diamond crystal. Crystals having a nearly complete conversion of the nitrogen into NV centers should thus greatly improve the present performance of our device. Note that the hyperfine coupling to the nuclear spin of ^{14}N could be turned into a useful resource if quantum information was transferred from the electron spin to the nuclear spin degree of freedom, which has much narrower linewidth. Finally, refocusing techniques borrowed from quantum memories in the optical domain [29] should also lead to increase in the storage time by 2 orders of magnitude.

In conclusion our experiments bring a proof of concept of a spin-based quantum memory for superconducting qubits. In a longer-term perspective, they open the way to the implementation of genuine quantum lab on chips, where superconducting qubits would coherently interact with electron and nuclear spins as well as optical photons.

We acknowledge useful discussions with K. Moelmer, F. Jelezko, J. Wrachtrup, D. Twitchen, and within the Quantronics group, and technical support from P. Sénat,

P.-F. Orfila, T. David, J.-C. Tack, P. Pari, P. Forget, and M. de Combarieu. We acknowledge support from European project Solid, ANR projects Masquelspec and QINVC, C'Nano, Capes, and Fondation Nanosciences de Grenoble.

Note added.—After redaction of this work, a related work reporting the coupling of a flux qubit to an ensemble of NV centers was published [30].

[1] C. F. Roos *et al.*, Phys. Rev. Lett. **92**, 220402 (2004).
[2] G. Balasubramanian *et al.*, Nature Mater. **8**, 383 (2009).
[3] L. DiCarlo *et al.*, Nature (London) **467**, 574 (2010).
[4] M. Neeley *et al.*, Nature (London) **467**, 570 (2010).
[5] J. A. Schreier *et al.*, Phys. Rev. B **77**, 180502 (2008).
[6] H. Paik *et al.*, arXiv:1105.4652 [Phys. Rev. Lett. (to be published)].
[7] A. Wallraff *et al.*, Nature (London) **431**, 162 (2004).
[8] A. D. O'Connell *et al.*, Nature (London) **464**, 697 (2010).
[9] M. Neeley *et al.*, Nature Phys. **4**, 523 (2008).
[10] A. Imamoglu, Phys. Rev. Lett. **102**, 083602 (2009).
[11] J. H. Wesenberg *et al.*, Phys. Rev. Lett. **103**, 070502 (2009).
[12] D. Marcos *et al.*, Phys. Rev. Lett. **105**, 210501 (2010).
[13] W. L. Yang, Z. Q. Yin, Y. Hu, M. Feng, and J. F. Du, Phys. Rev. A **84**, 010301 (2011).
[14] Y. Kubo *et al.*, Phys. Rev. Lett. **105**, 140502 (2010).
[15] D. I. Schuster *et al.*, Phys. Rev. Lett. **105**, 140501 (2010).
[16] R. Amsuss *et al.*, Phys. Rev. Lett. **107**, 060502 (2011).
[17] H. Wu *et al.*, Phys. Rev. Lett. **105**, 140503 (2010).
[18] Y. Kubo *et al.*, arXiv:1109.3960.
[19] F. Jelezko, T. Gaebel, I. Popa, A. Gruber, and J. Wrachtrup, Phys. Rev. Lett. **92**, 076401 (2004).
[20] S. Felton *et al.*, Phys. Rev. B **79**, 075203 (2009).
[21] See Supplemental Material at http://link.aps.org/supplemental/10.1103/PhysRevLett.107.220501 for details and five supplementary figures.
[22] J. Koch *et al.*, Phys. Rev. A **76**, 042319 (2007).
[23] F. Mallet *et al.*, Nature Phys. **5**, 791 (2009).
[24] M. Sandberg *et al.*, Appl. Phys. Lett. **92**, 203501 (2008).
[25] A. Palacios-Laloy *et al.*, J. Low Temp. Phys. **151**, 1034 (2008).
[26] M. Hofheinz *et al.*, Nature (London) **454**, 310 (2008).
[27] I. Diniz *et al.*, arXiv:1101.1842.
[28] Z. Kurucz, J. H. Wesenberg, and K. Molmer, Phys. Rev. A **83**, 053852 (2011).
[29] A. I. Lvovsky, B. C. Sanders, and W. Tittel, Nat. Photon. **3**, 706 (2009).
[30] X. Zhu *et al.*, Nature (London) **478**, 221 (2011).